Entropy, chaos, and excited-state quantum phase transitions in the Dicke model

C. M. Lóbez and A. Relaño

Departamento de Física Aplicada I and GISC, Universidad Complutense de Madrid, Av. Complutense s/n, 28040 Madrid, Spain

(Received 21 April 2016; revised manuscript received 8 July 2016; published 26 July 2016)

We study nonequilibrium processes in an isolated quantum system—the Dicke model—focusing on the role played by the transition from integrability to chaos and the presence of excited-state quantum phase transitions. We show that both diagonal and entanglement entropies are abruptly increased by the onset of chaos. Also, this increase ends in both cases just after the system crosses the critical energy of the excited-state quantum phase transition. The link between entropy production, the development of chaos, and the excited-state quantum phase transition is more clear for the entanglement entropy.

DOI: 10.1103/PhysRevE.94.012140

I. INTRODUCTION

The relation between statistical mechanics and the underlying microscopic dynamics is still an object of discussion. During the past couple of years, the development of experimental techniques allowing us to manipulate isolated quantum systems with a high degree of accuracy and control has motivated both experimental and theoretical research in this area [1,2]. In particular, the consequences of performing a quench—a sudden change in the external parameters of the Hamiltonian—have been largely explored, focusing on different fundamental open questions: the process of thermalization [3–5], the irreversibility arising from nonequilibrium dynamics [6–9], or the consequences of crossing critical points [10–12], just to cite a few. This paper follows the same line of research. We rely on the paradigmatic Dicke model [13] to study how entropy and entanglement are produced by a quench when the dynamics is affected by the onset of chaos and the presence of excited-state quantum phase transitions (ESQPTs). Our main conclusion is that all these phenomena are closely connected. Entropy production and entanglement are enhanced by the emergence of chaos and, though in a less clear way, by the presence of an ESQPTs.

In the macroscopic realm, irreversibility, the corresponding increase in entropy, and a number of statements about the work lost as a consequence of a process are equivalent [14]. However, the situation is totally different in a (small) isolated quantum system following unitary time evolution. The energy dissipated or lost due to a nonequilibrium process can be calculated unequivocally. However, the von Neumann entropy of the system, $S = -\mathrm{Tr}\rho\log\rho$, is always constant; it does not provide a microscopic basis for the Second Law. In other words, any time-dependent process $H(t)$ in any isolated quantum system keeps all the information about the initial state, and hence no entropy is produced as a consequence of it.

Recently, a number of ways to solve this problem have been explored. One consistent alternative relies on the diagonal entropy [15]. If the time-dependent wave function of a system following a nonequilibrium process is written $|\psi(t)\rangle = \sum_n C_n(t)|E_n(t)\rangle$, where $|E_n(t)\rangle$ are the instantaneous eigenstates of the system, and $H(t)|E_n(t)\rangle = E_n(t)|E_n(t)\rangle$, the diagonal entropy is defined as $S_d = -\sum_n |C_n(t)|^2 \log |C_n(t)|^2$. It can be understood as a natural consequence of the equilibration process that any isolated quantum system undergoes after a change in its external parameters—the process after which the state $|\psi(t)\rangle$ *relaxes* to an equilibrium mixed state, $\rho_{\mathrm{eq}} = \lim_{T\to\infty}\int_0^T dt\,|\psi(t)\rangle\langle\psi(t)|$, around which it fluctuates for the majority of the time [16]. As a consequence of the long-time average, the nondiagonal elements of ρ_{eq} vanish, and hence ρ_{eq} reduces to a diagonal mixed state, $\rho_{\mathrm{eq}} = \sum_n |C_n|^2|E_n\rangle\langle E_n|$. So, the diagonal entropy can be understood as the von Neumann entropy of this effective equilibrium state, resulting from dephasing. This entropy shares a number of important properties with the thermodynamic entropy. For example, in a time-dependent process $H(t)$, S_d only remains constant in the adiabatic limit; the adiabatic theorem forbids transitions between the different instantaneous eigenstates, so the coefficients $C_n(t)$ only acquire phases during the whole process. Furthermore, ρ_{eq} is expected to provide a good description of any experiment performed over the system; if the system thermalizes, the effective equilibrated state, ρ_{eq}, is expected to reproduce the expected values of physical observables, $\langle O\rangle \sim \mathrm{Tr}(O\rho_{\mathrm{eq}})$. Unfortunately, the diagonal entropy also suffers from some important limitations. For example, it changes immediately after a sudden quench $H(\lambda_i) \longrightarrow H(\lambda_f)$, where λ is an external control parameter of the Hamiltonian—it changes as soon as the quench is completed, not after the corresponding relaxation time. Hence, if the system undergoes a very fast cycle $H(\lambda_i) \longrightarrow H(\lambda_f) \longrightarrow H(\lambda_i)$, with a characteristic time much shorter that the relaxation time, this entropy first increases after the forward part of the cycle and then decreases again after the backward part. The reason is that the diagonal entropy S_d is equal to the von Neumann entropy of the effective equilibration state ρ_{eq}, so it implicitly assumes that the relaxation has been completed.

Another relevant alternative can be found in the entanglement between the system under study and its environment [17]. The most distinctive feature of entanglement, namely that none of the parts of an entangled system exists as an individual subsystem, has been used to link the Second Law and the unitary quantum evolution [7,18–20]. Let us consider that we are dealing with a global pure state, describing what we call the *universe*, that evolves unitarily under a certain global Hamiltonian H. All the information about this global state is conserved by the time evolution, and thus it has no entropy—despite the fact that it remains close to the effective relaxed state ρ_{eq} for the majority of the time. However, this being true, all of the possible experiments we can perform over

this global state are restricted to a small part of it—what we call the *system*. In addition, due to the entanglement between the different parts of the global pure state, we lack a relevant piece of information regarding the possible outcomes of our experiments, information that is encoded in the (inaccessible) correlations between the system and the rest of the universe—what we call the *environment*. Therefore, from the results of all of our possible experiments, we infer that our system is in a mixed state, it follows a nonunitary time evolution, and it has a (thermodynamic) entropy growing in time. In other words, quantum correlations between the system and its environment mean that there is an objective and unavoidable loss of information about the state of the system, and thus these correlations may be ultimately responsible for the Second Law. Indeed, these quantum correlations have been shown to give rise to canonical states in small parts of large and globally isolated quantum system [18]. Also, entanglement between the different parts of such systems has been identified as the mechanism leading to thermalization [19,20]. In addition, the corresponding entanglement entropy has been shown to split in reversible and irreversible contributions, the last of which grows as a consequence of the unitary evolution, provided that the initial condition is a separable mixed state [7]. So, as a promising alternative for the thermodynamic entropy, we can consider the reduced density matrix of the system after tracing out all the environmental degrees of freedom, $\rho_S(t) = \mathrm{Tr}_E|\psi(t)\rangle\langle\psi(t)|$, and its corresponding von Neumann entropy, $S_{\mathrm{ent}} = -\mathrm{Tr}_S\rho_S(t)\log\rho_S(t)$, which always depends explicitly on time.

The aim of this work is to explore the behavior of both diagonal and entanglement entropies in the paradigmatic Dicke model [13]. As we have pointed out before, it is reasonable to expect that both the effective equilibrated state, ρ_{eq}, from which we obtain the diagonal entropy S_d, and the reduced density matrix, ρ_S, giving rise to the entanglement entropy S_{ent}, provide a good description of the experiments performed in the system (see below for a precise description of what we call the system and what we call the environment), so it is logical to expect that both entropies account for the irreversibility inherent in a nonequilibrium process. We have chosen the Dicke model because of the following reasons: (i) it is experimentally accessible, by means of both a superfluid gas in an optical cavity [21] and superconducting circuits [22]; (ii) it is naturally split into two parts: a finite number of atoms (the *system*) and an infinite number of photons (the *environment*); and (iii) its spectrum has a very rich structure, showing both QPTs and ESQPTs [23–25], and a transition from integrability to chaos as a function of the energy [26,27].

After a stringent numerical study, we came to the following conclusions. Both diagonal and entanglement entropies are abruptly increased in the surroundings of the critical energy of the ESQPT, E_c, a region in which the system transits from almost integrable to fully chaotic dynamics. A possible explanation is that a number of approximately conserved quantities holding below the onset of chaos restrict the dynamics of the system, making the entropy increase less than expected in this region. It is also worthwhile to stress that diagonal and entanglement entropies do not behave in the same way. A tiny quench is enough to increase the first one; nonadiabatic transitions resulting from the quench spread the final energy distribution over many different eigenstates and give rise to a large value of the diagonal entropy, regardless of the approximated conservation rules holding below the onset of chaos. On the contrary, entanglement is almost zero until the system approaches the critical energy of the ESQPT and enters in the region in which the chaotic behavior starts. So, the behavior of these entropies is determined by different physical mechanisms. Diagonal entropy responds to any nonadiabatic transition between energy levels, providing a good estimate of irreversibility after the system is equilibrated in its final state. Entanglement entropy is more sensitive to structural changes in the eigenstates of the final Hamiltonian, and in particular to the mechanisms expected to lead the system to a final thermal state. Hence, from a thermodynamic point of view, diagonal entropy is more adequate because it is the only measure that captures the consequences of all the nonadiabatic transitions between energy levels; however, as we have pointed above, it is not useful to derive a time-dependent entropy $S(t)$, supporting the Second Law. On the other hand, entanglement entropy does increase in time, at least for large enough quenches; however, it does not account for all the irreversible changes.

The rest of the paper is organized as follows. In Sec. II we present the Dicke model, discuss its main features, and describe the process through which we obtain the results. In Sec. III we show the main results of the paper. Finally, in Sec. IV we summarize our main conclusions.

II. MODEL AND PROTOCOL

A. The Dicke model

The Dicke model [13] describes the coherent interaction of N two-level atoms of splitting ω_0 with a single bosonic mode of frequency ω. Considering that each atom has a ground state, $|g_i\rangle$, and an excited state, $|e_i\rangle$, the Dicke Hamiltonian can be written in terms of 1/2-spin operators, $J^{(i)}_{\pm,z}$, as $J^{(i)}_- = |g_i\rangle\langle e_i|$, $J^{(i)}_+ = |e_i\rangle\langle g_i|$, and $S^{(i)}_z = (1/2)(|g_i\rangle\langle g_i| + |e_i\rangle\langle e_i|)$. This formalism gives rise to

$$H = \omega_0 J_z + \omega a^\dagger a + \frac{2\lambda}{\sqrt{N}} J_x(a^\dagger + a), \tag{1}$$

where λ is the coupling constant, $a^\dagger$ and a are the creation and annihilation operators of photons, and $J = (J_x, J_y, J_z)$ is the total spin. This Hamiltonian has two main conserved quantities. The first quantity is J^2, which divides the Hamiltonian in diagonal blocks; in this paper, we restrict ourselves to $J = N/2$, which is enough to deal with the recent experimental realizations [21,22]. Second, due to the invariance of H under $J_x \to -J_x$ and $a \to -a$, $\Pi = \exp(i\pi[J + J_z + a^\dagger a])$ is also a conserved quantity. As this is a discrete symmetry, Π has only two different eigenvalues, $\Pi|E_i,\pm\rangle = \pm|E_i,\pm\rangle$, and it is usually called *parity*.

Despite the fact that it was formulated more than 60 years ago, the Dicke model is currently an object of intense research. First, it can be realized in a system more widely than cavity QED, for which it was originally formulated. Second, it shows a very rich behavior, including several kinds of phase transitions, and dynamics ranging from fully integrability to chaos. Third, it can be very well approximated by means of

a semiclassical model, at least in the thermodynamic limit $N \to \infty$.

The full version of the Dicke Hamiltonian, including all the possible values of J^2, shows a thermal phase transition if $\lambda > \sqrt{\omega\omega_0}/2$ [28–30]. However, if only the $J = N/2$ sector is considered, the transition disappears [31]. In this case, which is the one we are dealing with in this work, the only remainder of the transition occurs at $\lambda_c = \sqrt{\omega\omega_0}/2$, where the system undergoes a second-order QPT that separates the so-called normal phase ($\lambda < \lambda_c$) from the superradiant phase ($\lambda > \lambda_c$) [32].

This QPT has been linked to a singular behavior of the entanglement between the atoms and the radiation field [33], implying that an adiabatic evolution from the ground state of the system results in an abrupt increase of the entanglement at the critical coupling. It has also been related to the emergence of chaos [32]. Nevertheless, recent results show that the chaotic behavior in the Dicke model follows a more complex pattern [26,27,34]. For very low values of the coupling constant, $\lambda \ll \lambda_c$, the Dicke model behaves like a fully integrable system, despite the fact that the only integrable limit is $\lambda = 0$. However, for $\lambda \lesssim \lambda_c$ the system exhibits chaos, despite the fact that it is still in the normal phase. In this region, and also if $\lambda > \lambda_c$, the degree of chaos increases with energy. (See below for a more complete discussion about this fact.)

During the past few years, another kind of quantum phase transition has been studied in the Dicke model. For $\lambda > \lambda_c$, the QPT propagates to excited states, giving rise to an ESQPT at a critical energy $E_c = -J\omega_0$ [26,35,36]. The ESQPT has been linked to singularities in the derivatives of the density of states and some representative observables, such as J_z [36], and to a critical behavior in the relaxation process after a quench [35]. It has also been suggested that the ESQPT induces the development of chaos [26,37], but the current results are far from conclusive [27]. Finally, another relevant feature of the ESQPT is that it can induce symmetry-breaking equilibrium states [38,39]. If $\lambda > \lambda_c$ and $E < E_c$, all the energy levels are doubly degenerate in the thermodynamic limit. The main dynamical consequence of this fact is that symmetry-breaking observables, such as J_x, can relax to $J_x \neq 0$. On the contrary, if $\lambda < \lambda_c$ or if $E > E_c$ in the superradiant region, J_x always fluctuates around zero.

B. Protocol

All the results we show in this paper are based on the same procedure. We consider the ensemble of atoms to be the *system*, $H_S = \omega_0 J_z$; the radiation field is the *environment*, $H_E = \omega a^\dagger a$; and an interaction between them given is by $H_{\rm int} = 2\lambda J_x(a^\dagger + a)/\sqrt{N}$. The unitary time evolution of any pure state $|\psi(0)\rangle$ is given by $|\psi(t)\rangle = \mathcal{U}(t)|\psi(0)\rangle$, where $\mathcal{U}(t)$ is the unitary evolution operator, which can be obtained from Eq. (1). Exact calculations are accessible for current computational capabilities up to $N \sim 50$, and hence both diagonal and entanglement entropies can be numerically obtained. For the first one, we write the time-dependent wave function in the instantaneous eigenbasis, $|\psi(t)\rangle = \sum_n C_n(t)|E_n(t)\rangle$, and we take $S_d = -\sum_n |C_n(t)|^2 \log |C_n(t)|^2$. The entanglement entropy is obtained by tracing out the photonic degrees of freedom, $\rho_S(t) = {\rm Tr}_E[|\psi(t)\rangle\langle\psi(t)|]$, and taking $S_{\rm ent}(t) = -{\rm Tr}[\rho_S(t)\log\rho_S(t)]$. It is worthwhile to stress that, due to the correlations between atoms and photons, $\rho_S(t)$ does not follow a unitary time evolution, and thus $S_{\rm ent}(t)$ is explicitly time-dependent. Furthermore, this entropy has been shown to behave in the same qualitative way as other entanglement measures, at least for the ground state of this system [33].

Our main objective is to explore the consequences of a highly nonequilibrium process by suddenly changing the external parameter from λ_i to λ_f. This procedure is very easy to simulate, because the corresponding Hamiltonian does not depend explicitly on time; the exact time evolution comes directly from the final value of the coupling constant λ_f, $|\psi(t)\rangle = e^{iH(\lambda_f)t}|\psi(0)\rangle$, where the initial condition $|\psi(0)\rangle$ is the ground state of the system at the initial value of the coupling constant λ_i. We consider $\omega = \omega_0 = \hbar = 1$ throughout this paper. Also, we always take $\lambda_i > \lambda_f > \lambda_c$ in order to explore the complete phase diagram of the Dicke model (see [38] for details).

Another advantage of this procedure is that the ground state is very well described by a separable coherent state, $|\mu,\nu\rangle = |\mu\rangle \otimes |\nu\rangle$ [40], where

$$|\mu\rangle = (1+\mu^2)^{-J} \exp(\mu J_+)|J,-J\rangle, \tag{2}$$

$$|\nu\rangle = \exp(-\nu^2/2)\exp(\nu a^\dagger)|0\rangle, \tag{3}$$

correspond to the atomic and the bosonic parts of the state, respectively. The precise values of both parameters for a certain coupling constant λ_i are obtained by minimizing the energy surface $\langle\mu,\nu|H(\lambda_i)|\mu,\nu\rangle$,

$$\mu = \pm\sqrt{\frac{\lambda_i^2-\lambda_c^2}{\lambda_i^2+\lambda_c^2}}, \qquad \nu = \mp\frac{\sqrt{2J}}{\omega}\frac{\sqrt{\lambda_i^4-\lambda_c^4}}{\lambda_i}, \tag{4}$$

considering that we are always in the superradiant phase $\lambda_i > \lambda_c$. Furthermore, as in this phase ($\lambda > \lambda_c$) the ground state is always degenerate, any linear combination of the previous coherent states is also a valid ground state,

$$|\mu,\nu\rangle = \frac{\alpha|\mu_+\rangle \otimes |\nu_-\rangle \pm \beta|\mu_-\rangle \otimes |\nu_+\rangle}{\sqrt{|\alpha|^2+|\beta|^2}}, \tag{5}$$

where the subindex $+$ ($-$) indicates positive (negative) values in (4). Throughout this work, we restrict ourselves to the case $\alpha = 1$, $\beta = 0$. As this is a product state, all of the entanglement observed in the final equilibrium state is produced by the nonequilibrium process. Similar qualitative results are obtained for other values for α and β (not shown). The only difference is that the generic state in (5) is still entangled, thus its initial value for $S_{\rm ent}$ is not zero; a straightforward calculation shows that $S_{\rm ent}(0) = \log(|\alpha|^2+|\beta|^2) - \frac{1}{|\alpha|^2+|\beta|^2}(|\alpha|^2\log|\alpha|^2 + |\beta|^2\log|\beta|^2)$. Initial states with $\alpha = 1/\sqrt{2}$ and $\beta = \pm 1/\sqrt{2}$ are particularly interesting because they have well-defined positive or negative parity; in both cases, $S_{\rm ent}(0) = \log 2$. Note that for all these situations, $S_d(0) = 0$, since we always start the time evolution from the ground state.

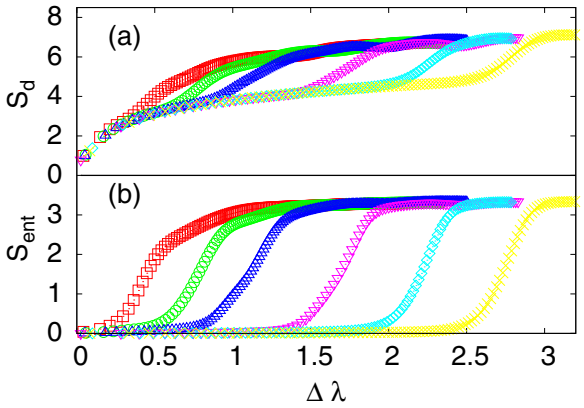

FIG. 1. Diagonal entropy S_d (a) and entanglement entropy $S_{\rm ent}$ (b) for a system with $N = 30$ atoms and different values for the final coupling constants, λ_f. Results are shown as a function of the size of the quench, $\Delta\lambda = \lambda_i - \lambda_f$. Open symbols display the numerical results: squares (red), $\lambda_f = 0.9$; circles (green), $\lambda_f = 1.2$; upper triangles (blue), $\lambda_f = 1.5$; lower triangles (magenta), $\lambda_f = 2.0$; diamonds (cyan), $\lambda_f = 2.5$; and crosses (yellow), $\lambda_f = 3.0$.

III. NUMERICAL RESULTS

First, we study the behavior of the system with $N = 30$ atoms and different values of the final coupling constant. In Fig. 1 we show the results for the diagonal entropy [panel (a)] and the entanglement entropy [panel (b)]. Symbols show the numerical results for $\lambda_f = 0.9$, 1.2, 1.5, 2.0, 2.5, and 3.0 (see the caption for details). In all the cases, the diagonal entropy S_d increases rapidly from $S_d = 0$ (limit for quenches small enough to avoid nonadiabatic transitions), showing that a large number of energy levels become populated after small or moderate quenches; note that the entropy generated is the same for all the cases. Then, a second region appears. Above $\Delta\lambda \sim 0.4$, the curves for the different cases follow different paths. The entropy generated by the quench ending at $\lambda_f = 0.9$ continues to grow with the same trend, whereas the increase of the others slows down, showing a sort of plateau. This plateau ends at a different value of $\Delta\lambda$ for each case, giving rise to a second rapidly growing region. The last part of all the cases consists of another slowly growing region, starting at different values of $\Delta\lambda$ for each case: the larger the λ_f, the larger is $\Delta\lambda$. Summarizing, the diagonal entropy grows following a complex path that depends on the final value of the coupling constant, λ_f.

Results for the entanglement entropy [Fig. 1(b)] also show a complex pattern. The first part of the plots consist of a region in which $S_{\rm ent} \sim 0$, that is, a region in which atoms and photons remain unentangled. The size of this region depends on λ_f: the larger λ_f, the larger is the quench $\Delta\lambda$ at which the entanglement entropy becomes significantly different from zero. Then, a rapidly growing region starts, very similar to the rapidly growing region of S_d after the intermediate plateau. In all the cases, $S_{\rm ent}$ grows from almost zero to almost its maximum value; in other words, atoms and photons change from almost pure to almost maximally entangled states in a narrow band of quench sizes. After this rapidly growing region, we reach a final regime in which the entanglement entropy is approximately constant and close to its maximum possible value, $S_{\rm ent} = \log 31$.

From these results, we infer the following conclusion. The entropy produced by the same process depends significantly on λ_f. As paradigmatic examples, we can compare the cases with $\lambda_f = 0.9$ and 3.0. In the first case, $S_{\rm ent}$ is roughly at its maximum for $\Delta\lambda \sim 1$. In the second one, the same quench size make atoms and photons remain almost unentangled, $S_{\rm ent} \sim 0$. Furthermore, the differences between S_d and $S_{\rm ent}$ are also significant. For example, the quench $\Delta\lambda \sim 1$ for the case $\lambda_f = 3.0$ entails $S_d \sim 3.5$, whereas $S_{\rm ent} \sim 0$. So, we conjecture that the entropy growth is related to structural changes in the spectrum, and that the entanglement entropy is more sensitive to these changes.

In the superradiant phase ($\lambda > \lambda_c$), two main structural changes occur above the ground state: the onset of chaos and an ESQPT. Recent results suggest that both phenomena are related (see [26] for the Dicke model and [37] for an atom-molecule gas), but it seems that they do not take place at the very same energy [27]. In any case, the distance between the ground state and the region in which both the ESQPT and the onset of chaos take place [26,27,38] increases with λ_f, indicating that the size of a quench $\Delta\lambda$ leading to this region also increases. Hence, it is logical to look for a connection between the rapidly growing region for both S_d and $S_{\rm ent}$, the onset of chaos, and the ESQPT.

A. Onset of chaos

Quantum chaos can be detected by means of several procedures. Most of these procedures are related to spectral statistics, that is, to the statistical properties of the sequence of energy levels [41]. An alternative approach has been used during the past few years to study how the degree of chaos changes with the excitation energy, a problem that is closely related to the one we are dealing with [42]. It was proposed around 30 years ago by Peres [43]. Basically, it consists of drawing the expected value of a representative observable [44] in every eigenstate in terms of the corresponding energy. If the system is fully chaotic, the plot shows no structure. On the contrary, if the system is integrable the plot is ordered in a regular lattice, due to the underlying integrals of motion. Such plots are usually called *Peres lattices*.

In Fig. 2 we represent a Peres lattice for a case with $N = 30$ and $\lambda_f = 2.5$. We have chosen the number of photons, $a^\dagger a$, as a representative observable. Together with the numerical points, we plot the critical energy of the ESQPT ($E_c/J = -1$) as a vertical dashed (green) line. Below $E/J \sim -4$, the lattice is regular. The values $\langle E_n|a^\dagger a|E_n\rangle$ are distributed in bands, each one following a different linear trend. Dotted lines in Fig. 2 represent these linear trends, obtained by least-squares fits to the corresponding sets of points. Around $E/J \sim -4$, some bands start to deviate from their linear trends, and above the critical energy of the ESQPT, $E/J = -1$, all the points distribute randomly. Thus, we can conclude that the transition from integrability to chaos happens in this interval.

In addition to the identification of quantum chaos, Peres lattices are also of interest to study the process of thermalization in isolated quantum systems. The eigenstate thermalization hypothesis (ETH) [5] states that an isolated quantum system

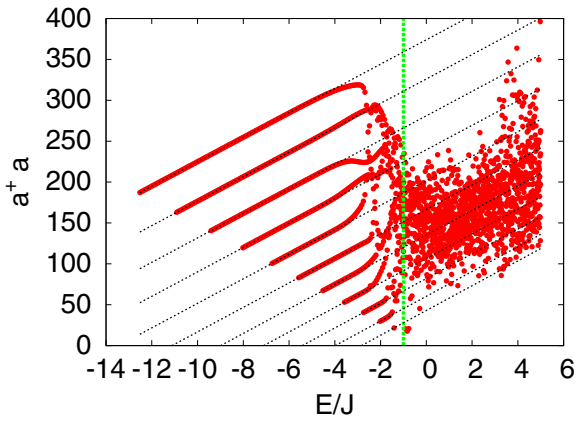

FIG. 2. Peres lattice for a system with $\lambda_f = 2.5$ and $N = 30$. Points (red) represent $\langle E_n|a^\dagger a|E_n\rangle$ vs the energy E_n/J of the eigenvector $|E_n\rangle$. The vertical dashed line (green) displays the critical energy of the ESQPT, $E_c/J = -1$. Black dashed lines show a visual guide to identify the regular pattern in the low-lying region of the spectrum, consisting of *bands*. These lines are obtained by means of a linear fit to the points in the corresponding band.

thermalizes if the expected values of physical observables are approximately the same in all the states within a small energy window ΔE. This fact entails that the expected value of any physical observable in a single eigenstate equals the microcanonical average, and therefore the system behaves as in thermal equilibrium independently of its actual probability distribution $P(E_n)$ [2–5]. In our case, this requirement is not fulfilled for $E/J < -4$; $\langle E_n|a^\dagger a|E_n\rangle$ changes dramatically from band to band, and hence we cannot expect a thermal behavior in this region. On the contrary, above the critical energy of the ESQPT, $\langle E_n|a^\dagger a|E_n\rangle$ fluctuates randomly around its average value. The width of the corresponding distribution is large, but we can expect that its relative size decreases with the number of atoms N, giving rise to thermalization in larger systems.

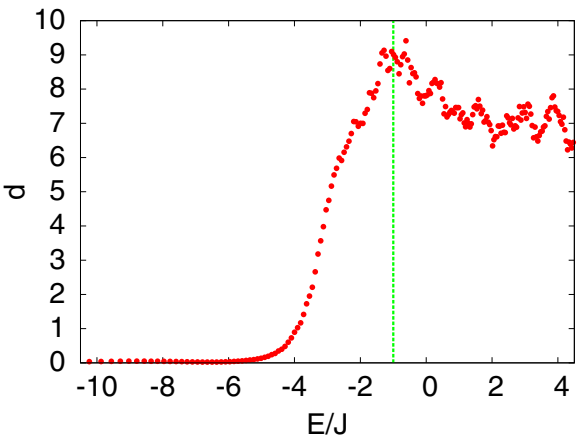

FIG. 3. Distance d between the points in the Peres lattice of Fig. 2 and their closest linear trend, averaged over $\Delta = 100$ consecutive points. The vertical dashed line (green) represents the critical energy of the ESQPT, $E/J = -1$.

A quantitative analysis is presented in Fig. 3, which has been constructed in the following way. First, we compute the distance d between every point $\langle E_n|a^\dagger a|E_n\rangle$ in the lattice and its closest linear trend. Second, we average the distances obtained over a fixed number of eigenstates, Δ. Finally, we represent the averaged d versus the average energy of the corresponding eigenstates. The results provide a measure of how ordered the lattice is in the neighborhood of a given energy E. If d is close to zero, the lattice exhibits a very regular pattern, and hence the system is almost integrable at the corresponding energy; if it is clearly different from zero, the system is far from integrability. Results plotted in Fig. 3 have been obtained with $\Delta = 100$. The distance d remains very close to zero up to energies around $E/J \sim -4$. Then, it increases rapidly up to its maximum, which remarkably happens around the critical energy of the ESQPT, $E/J \sim -1$. Finally, the distance d decreases a bit and oscillates around a certain value. So, we conclude that chaos emerges clearly below E_c, as was pointed out in [27], but the critical energy still plays a prominent role—results in Fig. 3 suggest that the system is fully chaotic above the ESQPT. It is worth noting that the distance d behaves in a similar way to the entropies shown in Fig. 1, especially S_{ent}: both d and S_{ent} remain close to zero within a certain range, and then they experience an abrupt increase. Although we do not show the numerical results, we have checked that this parallelism also holds for other values of the final coupling constant λ_f; for example, if $\lambda_f = 0.9$, the transition to chaos starts at very low excitation energies. Therefore, it is logical to expect a sort of link between the entropy generated by a quench and the development of chaos in the Dicke model.

With the aim of going deep into this possible link, we study the dynamical consequences of chaos in the Dicke model. We first analyze how the shape of the final energy distribution is affected by the onset of chaos. In Fig. 4 we plot the final energy distribution for a system with $N = 30$ and $\lambda_f = 2.5$, after different quenches (see the caption for details). Panels (a) and (b) are representative of small quenches, keeping the final energy distribution in the low-lying part of the spectrum, that is, in the nonchaotic ordered region (see Figs. 2 and 3). Together with the distribution, we plot the energies at which the different bands displayed in Fig. 2 start as vertical dashed lines (green); in panels (a) and (b), we show the energies corresponding to the second, $E_2/J \sim -10.9$, and the third, $E_3/J \sim -9.4$, bands. We can see that the appearance of these bands entails qualitative changes in the energy distributions. In the region in which there exists only one band (between $E/J \sim -12.5$ and $E/J \sim -10.9$), all the eigenstates become populated after the quench. On the contrary, both panels (a) and (b) show that only one in every two eigenstates becomes populated in the region with two bands (between $E/J \sim -10.9$ and $E/J \sim -9.4$). Finally, in panel (b) we can also see that only one in every three eigenstates becomes populated in the region with three bands (above $E/J \sim -9.4$). This suggests that a sort of approximated conservation rule holds: as our initial state is the ground state of the same system with $\lambda_i > \lambda_f$, only the eigenstates belonging to the first band are populated as a consequence of the quench; transitions between different bands are approximately forbidden by this conservation law.

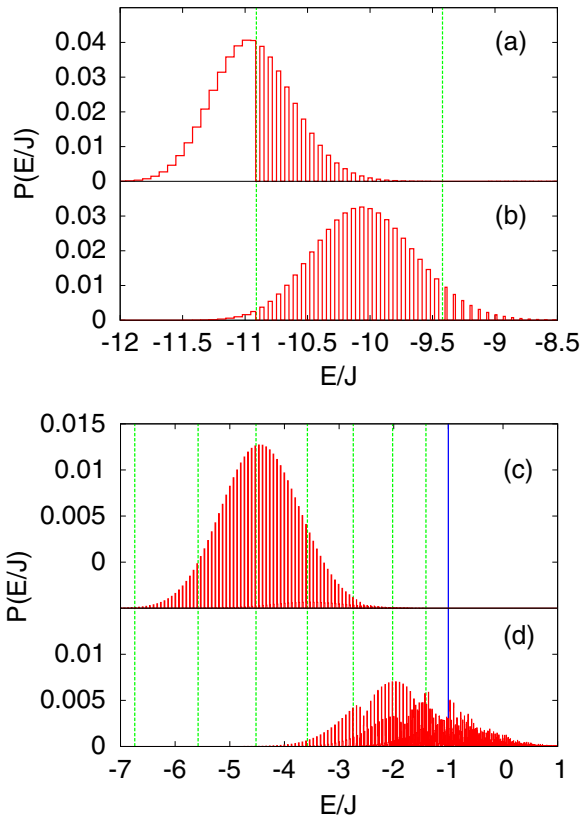

FIG. 4. Energy distributions $P(E_n)$ for a system with $N = 30$ and $\lambda_f = 2.5$, resulting from different quenches: (a) $\lambda_i = 3.4$; (b) $\lambda_i = 3.6$; (c) $\lambda_i = 4.5$; and (d) $\lambda_i = 4.8$. Vertical dashed lines (green) show the energies at which the different bands of Fig. 2 start. The vertical solid line (blue) shows the critical energy of the ESQPT, $E/J = -1$.

The results for large quenches, shown in panels (c) and (d), are different. The structure of the final eigenstate distribution is still regular in panel (c), though the approximated conservation rule suggested above is not so clearly seen. In fact, very small peaks appear around $E/J \sim -4.5$, giving rise to a secondary structure, suggesting that the approximated conservation rule starts to disappear. In panel (d), the distribution becomes erratic. In this case, the quench leads the system to the chaotic region. We can see that the complexity of the final distribution increases with energy, becoming random for energies above E_c. The secondary structure foreseen in panel (c) also appears around $E/J \sim -4$, and it becomes much more relevant around $E/J \sim -3$. After $E/J \sim -1.5$, we cannot distinguish between the main and the secondary structures, and the total distribution becomes totally erratic for energies above E_c. These results suggest that the approximated conservation rules, which are responsible for the regular behavior shown in panels (a) and(b), are destroyed by chaos. When the quench leads the system to the fully chaotic region, nonadiabatic transitions between all the energy levels are possible.

To obtain a more quantitative analysis of the transition from a regular pattern to random behavior in the eigenstate distribution after the quench, we proceed as follows. First, we select an intermediate quench, $\lambda_i = 4.0$, with the aim of spreading the wave function over both regular and chaotic

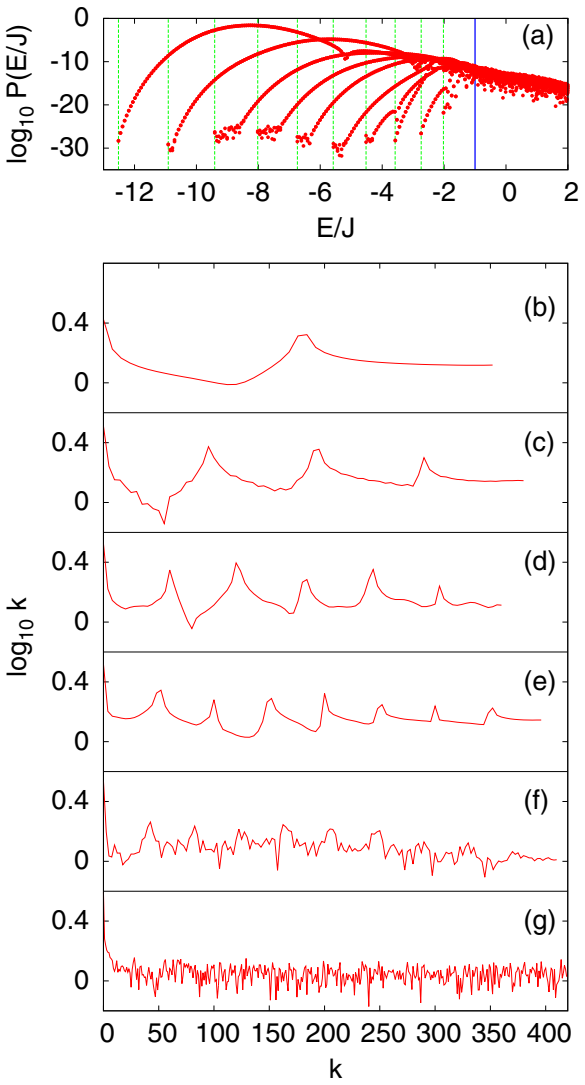

FIG. 5. (a) Logarithm of the final probability distribution, $P(E_n/J)$, for $\lambda_f = 2.5$ and $N = 30$. (b)–(g) Square modulus of the Fourier transform of the following series: (b) $x_n^{(2)}$, corresponding to eigenstates in the region with two bands, $-10.9 \lesssim E/J \lesssim -9.4$; (c) $x^{(4)}$, corresponding to eigenstates in the region with four bands, $-8.0 \lesssim E/J \lesssim -6.7$; (d) $x^{(6)}$, corresponding to eigenstates in the region with six bands, $-5.6 \lesssim E/J \lesssim -4.5$; (e) $x^{(8)}$, corresponding to eigenstates in the region with eight bands, $-3.6 \lesssim E/J \lesssim -2.7$; (f) $x^{(10)}$, corresponding to eigenstates in the region with ten or more bands, $-2.0 \lesssim E/J \lesssim -1.0$; (g) $x^{(11)}$, corresponding to eigenstates above the critical energy of the ESQPT, $-1.0 \lesssim E/J \lesssim 1.0$.

eigenstates. Second, we calculate the logarithm of the corresponding final energy distribution at $\lambda_f = 2.5$, obtaining a series $x_n = \log_{10} P(E_n/J)$. The logarithmic scale makes it possible to study patterns and periodicities in the final energy distribution even for very low occupation probabilities. The result is shown in Fig. 5(a) together with the energies at which the different bands start [as vertical dashed (green) lines] and the critical energy of the ESQPT [as a vertical solid (blue) line]. We see a clearly regular pattern for the low-lying eigenstates, as expected. But it is also worth noting that the previously discussed conservation rules are only

approximated; all the bands are significantly populated [45], though only the population of the eigenstates in the first band is relatively large, within a window around the expected final energy. Furthermore, we can see the first signatures of an irregular behavior between $E/J = -4$ and -3, though the plot becomes clearly noisy only above $E/J \sim -1.5$. From this plot, we get a quantitative analysis of regularities and patterns in the dynamics after the quench in the following way. We divide the series $x_n \equiv \log_{10} P(E_n/J)$ in different sequences, each one corresponding to a different region in Fig. 5(a): $x_n^{(1)}$ is the logarithm of the probability $P(E_n)$ of the eigenstates in the region with just one band, $-12.5 \lesssim E/J \lesssim -10.9$; $x_n^{(2)}$ is the same for the eigenstates in the region with two bands, $-10.9 \lesssim E/J \lesssim -9.4$; and so on. Finally, we obtain the square modulus of the Fourier transform of the sequences $x_n^{(i)}$. Results are also plotted in Fig. 5 for $x_n^{(2)}$, $x_n^{(4)}$, $x_n^{(6)}$, $x_n^{(8)}$, $x_n^{(10)}$, and $x_n^{(11)}$ (see the caption for details). In panels (b)–(e), we see that the number of peaks in the Fourier transform of $x_n^{(i)}$ coincides with the number of bands in the corresponding region of the spectrum. This is a consequence of the regular structure shown in panel (a) of the same figure. $x_n^{(2)}$ oscillates between the first (upper set of points) and the second (lower set of points) bands, and therefore the corresponding Fourier transform shows a peak in $k = 0$ and a second peak related to the frequency of these oscillations, which is more or less the same for the complete subsequence. Something similar happens with $x_n^{(4)}$. In this case, the signal oscillates between four different points, entailing three different frequencies, and the peak at $k = 0$. This scenario is broken in the last two panels. Panel (f) is in the region transiting from integrability to fully developed chaos, $-2.0 \lesssim E/J \lesssim -1.0$. Despite the fact that a number of peaks can still be distinguished, the signal is noisy. Finally, panel (g) shows the results for levels above the critical energy of the ESQPT, $-1.0 \lesssim E/J \lesssim 1.0$. In this case, we find no traces of peaks; the signal is compatible with a white noise, that is, with an uncorrelated sequence. These facts entail that the probability distribution $P(E_n)$ transits from a periodic structure, coming from the approximated conservation rules holding in the low-lying region of the spectrum, to a totally uncorrelated one, occurring in the fully chaotic region.

All these results show that the dynamics is strongly affected by the development of chaos; the final energy distribution, which is directly correlated with the diagonal entropy S_d, changes dramatically from the almost integrable to the fully chaotic regimes. The effects in the entropy generated by a quench are studied in Fig. 6. There, we show the diagonal entropy [panel (a)] and the entanglement entropy [panel (b)] for $N = 30$ and $\lambda_f = 2.5$ as a function of the final energy E/J. We also show the energies at which chaos starts, $E/J \sim -4$, as a vertical dashed (green) line, and the critical energy of the ESQPT, $E/J = -1$, as a vertical solid (blue) line. From the results, we can infer a neat correlation between the onset of chaos and the increase of both S_d and S_{ent}. In particular, this correlation is remarkable for the entanglement entropy S_{ent}; we can see impressive similarities between Fig. 3 and of Fig. 6(b). Hence, from the comparison of these two figures, we can conclude the following: (i) atoms and photons remain unentangled for quenches, keeping the system in the almost integrable region, characterized by a number of approximated conservation rules that prevent the majority of the nonadiabatic transitions between energy levels; (ii) the entanglement increases rapidly in the region transiting from integrability to chaos; and (iii) atoms and photons are almost yet maximally entangled after the system crosses the ESQPT and enters in the fully chaotic regime. It is worth mentioning that these facts reinforce the link between entanglement and thermalization [19,20]: S_{ent} starts to grow when the ordered pattern in $\langle a^\dagger a \rangle$ starts to disappear, that is, when the conditions for the ETH start to hold. We can expect that quenches leading the system to the low-lying region of the spectrum do not result in a thermal equilibrium state; approximated conservation rules prevent ETH, and the atomic and photonic parts of the system remain too uncorrelated for the emergence of canonical states [19]. On the contrary, quenches leading the system to the chaotic region, in particular to final energy values above the ESQPT, are expected to entail thermal behavior; no regularities in the final energy distribution are found, and the entanglement between the atomic and the photonic parts of the system is very large.

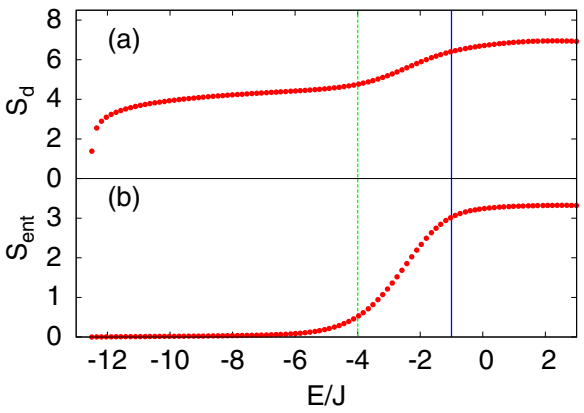

FIG. 6. Diagonal entropy S_d (a) and entanglement entropy S_{ent} (b) for a system with $N = 30$ atoms and different values for the final coupling constants, λ_f, as a function of the final energy E/J.

The diagonal entropy S_d is also linked to the onset of chaos, but not so strongly. Its fast growing region also coincides with the transition from integrability to chaos. We can interpret this result as a consequence of the breaking of the approximated conservation rules holding in the almost integrable region. When this transiting region is reached, a lot of nonadiabatic transitions become possible, spreading the final energy distribution over a much larger number of eigenstates, and largely increasing the diagonal entropy. However, S_d is also significantly larger than zero for quenches, leading the system to the almost integrable region. This fact entails that such quenches are irreversible, though they neither correlate atoms and photons nor lead the system to thermal behavior.

B. ESQPT

The results in the previous sections suggest that the emergence of chaos plays a prominent role in the entanglement between the atomic and the photonic part of the Dicke model. Notwithstanding, the ESQPT seems to be important, too. Results shown in Figs. 3, 5, and 6 suggest that the system becomes fully chaotic after crossing the critical energy of the ESQPT, atoms and photons become maximally entangled

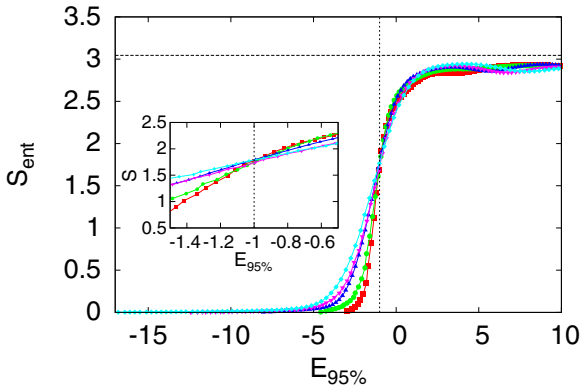

FIG. 7. Entanglement entropy $S_{\rm ent}$ for $N = 20$ and different values of λ_f as a function of $E_{95\%}$ (see the main text for details). Squares (red) correspond to $\lambda_f = 1.2$; circles (green) correspond to $\lambda_f = 1.5$; lower triangles (blue) correspond to $\lambda_f = 2.0$; lower triangles (magenta) correspond to $\lambda_f = 2.5$; and diamonds (cyan) correspond to $\lambda_f = 3.0$. The vertical dotted line shows the critical energy of the ESQPT, $E_c/J = -1$; the horizontal dashed line shows the maximum possible value for the von Neumann entropy, $S = \log 21$. The inset shows a zoom of the same results around $E/J = -1$.

roughly at the same point, and also the rapidly growing region of the diagonal entropy ends approximately at the same value. Since the results for $S_{\rm ent}$ are clearer than those for S_d (the entanglement entropy grows from zero to almost its maximum possible value in a very narrow energy window), we explore now the possible links between this magnitude and the ESQPT.

The results shown in Fig. 6 are not conclusive regarding the possible link between entanglement and the ESQPT. The development of chaos occurs within quite a wide energy window; hence, the fact that the final energy distribution is also wide does not constitute a problem. On the contrary, the ESQPT is a critical phenomenon taking place at a precise value of the energy, $E_c/J = -1$; thus, we can expect that its dynamical consequences become blurred if the final energy distribution is wide. To avoid this problem, we recalculate the consequences of the same quenches, though for a smaller system with $N = 20$ (to have more numerical points), and we study the entanglement entropy $S_{\rm ent}$ in terms of $E_{95\%}$. This is the energy value that fulfills $F(E \leqslant E_{95\%}) = 0.95$, where $F(E)$ is the cumulative probability distribution for the energy in a measurement. In other words, we plot the results versus the energy below which 95% of the energy distribution exists. This value has been selected to identify the point at which the system *touches* the critical point, that is, the point at which the fully chaotic phase starts to be significantly populated [46]. In Fig. 7, we plot the corresponding results for different values of the final coupling constant, λ_f (see the caption of Fig. 7 for details). In the inset, we plot a zoom of the same curves, centered at the critical energy $E_{95\%}/J = -1$. The main conclusion is that all five curves cross at the critical point $E_{95\%}/J \sim -1$, suggesting that this point plays a significant role in the dynamics of the entanglement entropy. Notwithstanding, this result is not as conclusive as the obtained results regarding the onset of chaos. More work is needed to separate the consequences of chaos and the ESQPT.

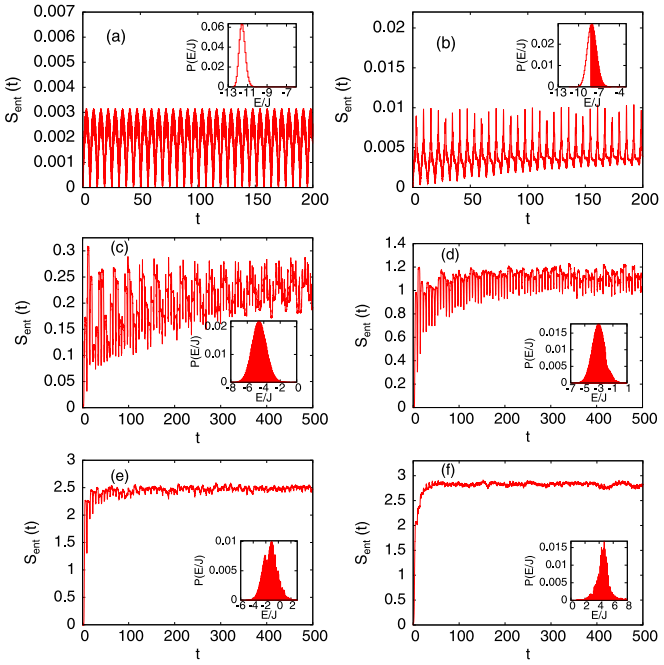

FIG. 8. Entropy production for a system with $N = 20$ atoms and $\lambda_f = 2.5$. Panel (a) corresponds to $\lambda_i = 3.0$; panel (b) to 4.0; panel (c) to 4.7; panel (d) to 4.9; panel (e) to 5.5, and panel (f) to 7.0. In the main part of the panels, red lines show $S_{\rm ent}$. In the insets, the final energy distribution is shown.

C. Entropy growth

As was discussed in the Introduction, one of the main differences between diagonal S_d and entanglement $S_{\rm ent}$ entropies is that the first one changes immediately after the quench, while the second one has a nontrivial time dependence, which can be related to the Second Law [7]. We explore here this time dependence.

In Fig. 8, we plot how the entanglement entropy $S_{\rm ent}$ grows after the quench. All the results are numerically obtained with $N = 20$ atoms and $\lambda_f = 2.5$. For the sake of clarity, we have selected a set of representative cases that give rise to final states with the following properties: panel (a), with $\lambda_i = 3.0$, shows a case in which only the first band of levels is populated; panel (b), with $\lambda_i = 4.0$, is clearly below the onset of chaos, though more of one band is populated; in panel (c), with $\lambda_i = 4.7$, levels within the transition from integrability to chaos are still populated, though almost all the energy distribution is below the critical energy of the ESQPT, $E/J = -1$; panel (d), with $\lambda_i = 4.9$, shows a case in which the final energy distribution *touches* the critical energy, and almost all is within the transiting region; in panel (e), with $\lambda_i = 5.5$, the energy distribution is roughly centered at the critical energy $E/J = -1$; and panel (f), with $\lambda_i = 7.0$, shows a case in which almost all the energy distribution is in the fully chaotic region. In panel (a), $S_{\rm ent}$ is periodic in time, oscillating from zero to a very small value. Panel (b) is very similar, though we can foresee a very small entropy growth. As both cases correspond to a final state in the low-lying regular region of the spectrum, we can conclude that almost no entanglement is produced under these circumstances, and

that the time dependence of the corresponding entropy is not related with the irreversibility produced by the quench. As we can see in both panels, the final energy distribution is wide, implying that a number of nonadiabatic transitions have occurred. The results plotted in Fig. 6(a) show that S_d is significantly larger than zero under these circumstances. So, these results make evident the different roles played by entanglement and diagonal entropies. Though the atomic part of the system remains almost pure, entailing no entanglement entropy, the nonzero value of the diagonal entropy indicates that we cannot revert the process. The system enters in the region transiting from integrability to chaos in panel (c). In this case, we can see that the main trend of $S_{\rm ent}$ is clearly increasing; in other words, the purity of the atomic system decreases in time. The qualitative behavior of panel (d) is very similar, though the final equilibrium value for $S_{\rm ent}$ is clearly larger, because the final energy distribution is in the transiting region. There is an abrupt increase of such equilibrium values between panels (d) and (e), that is, when the final energy distribution crosses the critical energy and enters in the totally chaotic region. Note that the curve in panel (e) reaches its final equilibrium value clearly earlier than the curve in panel (d), and that the relative weight of its fluctuations is much smaller. Finally, when almost all the energy distribution exists in the fully chaotic region, panel (f), fluctuations are even smaller, but the main trend of $S_{\rm ent}$ is very similar to the previous case.

From these results, we conclude that $S_{\rm ent}$ shows a main trend qualitatively, but not quantitatively, compatible with the Second Law. In addition to fluctuations, which are large due to the small sizes accessible to current computational capabilities, $S_{\rm ent}$ grows in time in a similar way to that shown in recent theoretical calculations for other systems [7] and experiments [20]. Starting from a separable state, and for quenches large enough, the atomic part of the system changes from a pure to a mixed state. However, this growth is only significant above the onset of chaos. When the state of the system remains within the low-lying regular part of the spectrum, the resulting entanglement entropy is very low, or even periodic in time, despite the fact that the final energy distribution has a finite width. In other words, below the onset of chaos, the nonadiabatic transitions resulting from the quench do not correlate the atomic and the photonic parts of the system. So, the entanglement entropy is not enough to characterize all the irreversible processes taking place in a globally isolated quantum system.

IV. CONCLUSIONS

In this paper, we have studied the entropy generated by a quench in an isolated quantum many-body system, the Dicke model, describing the interaction between a set of two-level atoms with a monochromatic radiation field. We have dealt with different magnitudes: the diagonal entropy, S_d, which can be understood as the von Neumann entropy of the final equilibrium state, $\rho_{\rm eq}$; and the entanglement entropy, $S_{\rm ent}$, which is the von Neumann entropy of the atomic part of the system, obtained by tracing out the photonic degrees of freedom. We have computed numerically the exact time evolution of the complete system, and we have derived both entropies from these exact results. We have arrived at the following main conclusions.

First, entropy production is largely increased by chaos. Small quenches, keeping the system in an almost integrable regime, entail a small value for the diagonal entropy S_d, and an almost zero value for the entanglement entropy $S_{\rm ent}$. On the contrary, large quenches, leading the system to a fully chaotic regime, entail very large values for both entropies. In particular, $S_{\rm ent}$ changes from almost zero to almost its maximum possible value in the same regime in which the final Hamiltonian changes from almost integrable to fully chaotic. It is worth mentioning that this fact is closely related to the transition from nonthermal to thermal behavior. In the almost integrable regime, the conditions of the eigenstate thermalization hypothesis (ETH), the mechanism responsible for thermalization in isolated quantum systems, does not hold, so we cannot expect that the system behaves according to standard thermodynamics. On the contrary, the ETH holds when the dynamics becomes fully chaotic, so we can expect that the system *forgets* all the details about its initial condition in this regime, giving rise to a thermal final equilibrium state. We have shown that the transition in the entanglement entropy $S_{\rm ent}$ is highly correlated with the transition from non-ETH to ETH scenarios. This result is compatible with recent experiments showing that the entanglement between different parts of a (small) quantum system is responsible for thermalization [20]. Regarding the diagonal entropy, we have shown that a similar transition also takes place, though the change is not so abrupt as for $S_{\rm ent}$. We conclude that the process becomes more irreversible when the system enters in the fully chaotic regime, because in the almost integrable regime there are a number of approximated conservation rules, limiting the amount of nonadiabatic transitions between energy levels.

Second, there is a subtle link between the entanglement entropy, $S_{\rm ent}$, and the presence of an excited-state quantum phase transition (ESQPT). We have shown that the critical energy of the ESQPT, E_c, is also a singular point regarding entanglement entropy production. However, this link is clearly weaker than the previous one, and it requires further research.

Finally, we have shown that the time dependence of $S_{\rm ent}$ agrees qualitatively with a thermodynamic entropy supporting the Second Law, but this agreement is not quantitatively correct. When the final state exists in the almost integrable regime, atoms and photons remain almost unentangled, though the process is irreversible, a certain amount of energy is dissipated, and the diagonal entropy S_d is significantly larger than zero. It is worthwhile to remark that this occurs in a regime in which thermalization is not expected, that is, in a regime in which standard thermodynamics does not work.

Summarizing, we have found a clear link between irreversibility and chaos in the Dicke model. Also, we have found some traces identifying a weaker link between entropy production and crossing the critical point of an ESQPT.

ACKNOWLEDGMENTS

This work has been partially supported by the Spanish Grants No. FIS2012-35316 and No. FIS2015-63770-P (MINECO/FEDER). C.M.L. is supported by the Spanish

MECD Program "Becas de Colaboración." A.R. thanks R. Puebla for enlightening discussions. C. M. L. thanks A. Alsina and D. Mendez-Gonzalez for useful advice that clarified the meaning of several topics.

[1] I. Bloch, J. Dalibard, and W. Zwerger, Rev. Mod. Phys. **80**, 885 (2008).
[2] A. Polkovnikov, K. Sengupta, A. Silva, and M. Vengalatore, Rev. Mod. Phys. **83**, 863 (2011).
[3] J. M. Deutsch, Phys. Rev. A **43**, 2046 (1991).
[4] M. Srednicki, Phys. Rev. E **50**, 888 (1994).
[5] M. Rigol, V. Dunjko, and M. Olshanii, Nature (London) **452**, 854 (2008).
[6] J. Gemmer, M. Michel, and G. Mahler, *Quantum Thermodynamics*, Lecture Notes in Physics Vol. 657 (Springer, Berlin, 2005).
[7] M. Esposito, K. Lindenberg, and C. Van den Broeck, New J. Phys. **12**, 013013 (2010).
[8] A. E. Allahverdyan and Th. M. Nieuwenhuizen, Phys. Rev. E **71**, 046107 (2005).
[9] R. Puebla and A. Relaño, Phys. Rev. E **92**, 012101 (2015).
[10] A. Polkovnikov, Phys. Rev. B **72**, 161201(R) (2005).
[11] W. H. Zurek, U. Dorner, and P. Zoller, Phys. Rev. Lett. **95**, 105701 (2005).
[12] M. A. de Avillez and D. Breitschwerdt, Proc. Int. Astro. Union **5**, 468 (2009).
[13] R. H. Dicke, Phys. Rev. **93**, 99 (1954).
[14] H. B. Callen, *Thermodynamics and an Introduction to Thermostatistics* (John Wiley & Sons, New York, 1985).
[15] A. Polkovnikov, Ann. Phys. (N.Y.) **326**, 486 (2011).
[16] P. Reimann and M. Kastner, New. J. Phys. **14**, 043020 (2012).
[17] R. Horodecki, P. Horodecki, M. Horodecki, and K. Horodecki, Rev. Mod. Phys **81**, 865 (2009); L. Amico, R. Fazio, A. Osterloh, and V. Vedral, *ibid.* **80**, 517 (2008).
[18] S. Popescu, A. J. Short, and A. Winter, Nat. Phys. **2**, 754 (2006).
[19] S. Khlebnikov and M. Kruczenski, Phys. Rev. E **90**, 050101(R) (2014).
[20] A. M. Kaufman, M. E. Tai, A. Lukin, M. Rispoli, R. Schittko, P. M. Preissm, and M. Greiner, arXiv:1603.04409.
[21] K. Baumann, C. Guerlin, F. Bennecke, and T. Esslinger, Nature (London) **464**, 1301 (2010).
[22] A. Mezzacapo, U. Las Heras, J. S. Pedernales, L. DiCarlo, E. Solano, and L. Lamata, Sci. Rep. **4**, 7482 (2014).
[23] P. Cejnar, M. Macek, S. Heinze, J. Jolie, and. J. Dobes, J. Phys. A **39**, L515 (2006).
[24] M. A. Caprio, P. Cejnar, and F. Iachello, Ann. Phys. (N.Y.) **323**, 1106 (2008).
[25] P. Stransky, M. Macek, and P. Cejnar, Ann. Phys. (N.Y.) **345**, 73 (2014).
[26] P. Pérez-Fernández, A. Relaño, J. M. Arias, P. Cejnar, J. Dukelsky, and J. E. García-Ramos, Phys. Rev. E **83**, 046208 (2011).
[27] M. A. Bastarrachea-Magnani, S. Lerma-Hernández, and J. G. Hirsch, Phys. Rev. A **89**, 032102 (2014).
[28] K. Hepp and E. H. Lieb, Ann. Phys. (N.Y.) **76**, 360 (1973).
[29] Y. K. Wang and F. T. Hioe, Phys. Rev. A **7**, 831 (1973).
[30] H. J. Carmichael, C. W. Gardiner, and D. F. Walls, Phys. Lett. A **46**, 47 (1973).
[31] M. A. Alcalde, M. Bucher, C. Emary, and T. Brandes, Phys. Rev. E **86**, 012101 (2012).
[32] C. Emary and T. Brandes, Phys. Rev. Lett. **90**, 044101 (2003); Phys. Rev. E **67**, 066203 (2003).
[33] N. Lambert, C. Emary, and T. Brandes, Phys. Rev. Lett. **92**, 073602 (2004).
[34] A. Altland and F. Haake, New. J. Phys. **14**, 073011 (2012).
[35] P. Pérez-Fernández, P. Cejnar, J. M. Arias, J. Dukelsky, J. E. García-Ramos, and A. Relaño, Phys. Rev. A **83**, 033802 (2011).
[36] T. Brandes, Phys. Rev. E **88**, 032133 (2013).
[37] A. Relaño, J. Dukelsky, P. Pérez-Fernández, and J. M. Arias, Phys. Rev. E **90**, 042139 (2014).
[38] R. Puebla, A. Relaño, and J. Retamosa, Phys. Rev. A **87**, 023819 (2013).
[39] R. Puebla and A. Relaño, Europhys. Lett. **104**, 50007 (2013).
[40] W.-M. Zhang, D. H. Feng, and R. Gilmore, Rev. Mod. Phys. **62**, 867 (1990).
[41] J. M. G. Gómez, K. Kar, V. K. B. Kota, R. A. Molina, A. Relaño, and J. Retamosa, Phys. Rep. **499**, 103 (2011).
[42] P. Stránský, P. Hruška, and P. Cejnar, Phys. Rev. E **79**, 066201 (2009).
[43] A. Peres, Phys. Rev. Lett. **53**, 1711 (1984).
[44] The original method by Peres is devoted to the study of the transition from integrability to chaos, by perturbing an integrable Hamiltonian H_0, giving rise to $H(\lambda) = H_0 + \lambda V$. If $\lambda = 0$, there exists at least one nontrivial integral of motion I commuting with the Hamiltonian, $[H, I] = 0$. This entails that, in this case, the plot of $\langle E_n|I|E_n\rangle$ vs the corresponding energy is regular. On the contrary, if $\lambda \neq 0$, I is no longer an integral of motion, and hence the order in the same plot is destroyed. For this reason, in the original Peres lattices, the chosen observable has to be an integral of motion in a certain limit, $\lambda = 0$. It is worth noting that in the observable we have chosen in Fig. 2, the number of photons $a^\dagger a$ is an integral of motion if $\lambda = 0$.
[45] As calculations are performed in double precision, coefficients up to 10^{-15}–10^{-16} in the expansion of the wave function in the eigenbasis of the final Hamiltonian λ_f are significant, entailing probabilities up to 10^{-30}–10^{-32}.
[46] The choice of $E_{95\%}$ is arbitrary; we could choose $E_{99\%}$, $E_{90\%}$, or any other value representing the tail of the distribution. We understand that 95% is somehow equivalent to a statistical significance $p = 0.05$.